American Journal of Energy Research, 2022, Vol. 10, No. 1, 1-8
Available online at http://pubs.sciepub.com/ajer/10/1/1
Published by Science and Education Publishing
DOI:10.12691/ajer-10-1-1

Design and Simulation of a Solar Brine Dryer for the Production of Sea Salt

Vincent Prodjinonto[1], Ayihaou Armand Djossou[1,2], Gérard Wilfried Adjahossou[1,3,*], Julien Adounkpe[3], Clément Ahouannou[1,3]

[1]Laboratory of Energetics and Applied Mechanics (LEMA), University of Abomey-Calavi
[2]Laboratory of Processes and Technological Innovation (LaPIT),
National Higher Institute of Industrial Technology (INSTI) of Lokossa
[3]Food Conservation by Utilizing Solar Energy for Drying-Republic of Benin (FOCUSED), University of Abomey-Calavi
*Corresponding author: agwilfried@gmail.com

Received September 08, 2022; Revised October 10, 2022; Accepted October 22, 2022

Abstract With a view to ensuring the sustainable development of Third World countries, the protection of mangroves is essential insofar as mangroves play an important role in the maintenance of ecosystems. Opting for sustainable development strategies and policies aimed at promoting the production of solar salt on tarpaulins in Africa will help achieve this objective while curbing the destruction of the mangrove. It is therefore for this purpose that the present research aims to develop a solar salt production device called solar brine dryer for the production of sea salt. The device is supported on the ground by a parallelepipedic granite block constituting the foundation of the whole and whose role is to store the heat and restore it in low sunlight. The side walls and the roof are made of polymethyl methacrylate (plexiglass). The different vertical faces are connected by posts which are made of aluminium. The device makes the production of salt sustainable and prevents any contamination due to contact with the sand. Also the results of simulation obtained thanks to the model of Luis and Jordan for the estimation of the solar irradiance and to the model of Rohwer for the calculation of the rate of evaporation, show that the device optimizes the production of salt with an average of 7.55 kg of salt per day in an area of 12 m^2 against an average production of 1.4 kg of salt per day in an area of 250 m^2 with the solar cover method.

Keywords: *conception, dryer, mangrove, plexiglass, salt, simulation, tarpaulin*

Cite This Article: Vincent Prodjinonto, Ayihaou Armand Djossou, Gérard Wilfried Adjahossou, Julien Adounkpe, and Clément Ahouannou, "Design and Simulation of a Solar Brine Dryer for the Production of Sea Salt." *American Journal of Energy Research*, vol. 10, no. 1 (2022): 1-8. doi: 10.12691/ajer-10-1-1.

1. Introduction

Salt is the support of many human activities, related to food, hygiene, body care [1]. Natural brine (sea water, salt spring) or artificial brine is transformed into salt. Artificial brine is obtained by the leaching of various elements (earth, sand) [2]. In Benin, according to the investigations carried out by the FOCUSED-Benin project, both types of brine are used for the production of salt. The latter is obtained from artificial brine by heating over a wood fire. But this very wood-intensive technique destroys the mangroves and at the same time impacts fisheries resources. The women were then introduced to the production of solar salt with natural brine: this is the case of salt production in the municipality of Sèmè-Kpodji. Indeed, the sea water is poured on tarpaulins called geomembranes, then thanks to the action of the sun and the wind there is evaporation of the water. But this time-consuming technique is very unproductive in terms of the quantity of salt produced (1.4 kg of salt per day after measurement during the investigations of the FOCUSED-Benin project) when a comparison is made with the yield of the traditional technique. In addition, this approach only takes place seasonally and the salt produced mixes with the sea sand because the geomembranes are exposed on the ground and in the open air. Our objective is therefore to set up a solar brine dryer using natural wind convection and solar radiation to produce sea salt. This system will solve many problems, namely: cases of illness due to prolonged exposure to fire and smoke on the one hand, fluctuating financial income and the precariousness of women producers on the other.

Several authors have tried to solve the problem of the preservation of the mangrove and the fish species that depend on it and at the same time that relating to the need for domestic and industrial salt. In 2010 Dossou and al [3] carried out a comparative study of the performance of traditional salt production equipment with a crystallizer on a tarpaulin and a solar seawater distiller developed and tested for the production of sea salt. The geomembrane solar crystallizer used in this case does not highlight the greenhouse effect. Moreover, in the rainy season, this crystallizer is unable to produce salt: the problem of irregularity in production still remains with this method.

In 2010, HALLOUFI studied the performance of a solar still by a solar pre-heating system for brackish water [4].

But the natural convection of the wind does not contribute to the evaporation of the brine because this distiller is hermetically sealed, so this study is different from ours.

Fatima Sow (2012) and UNIVERS SEL (1989) worked on the production of solar salt on a geomembrane while preserving the mangroves [5]. But this work cannot solve the problems of optimization and irregularity of salt production in the municipality of Sèmè-Kpodji because they do not take into account either protection of the system or a concentration device.

In 2019, BANI and PRODJINONTO designed a solar still for the mixed production of cooking salt and electricity in Benin [6]. But the operation of this distiller is not based on the natural convection of the wind to promote the evaporation of the brine.

Our device, based on the Rohwer model, combines natural convection and solar radiation to accelerate salt production. These two parameters allow the optimization of evaporation according to Rohwer (1931).

2. Material and Methods

2.1. Material

The device (see Figure 1) is a translucent frame made of Plexiglas with four side faces and a roof inclined at 15°C with respect to the horizontal plane in order to allow it to be self-cleaned [7]. The foundation is a granite paver whose role is to store the heat inside the device. It is ultimately a brine drying greenhouse. The different vertical faces are connected by posts which are made of aluminium.

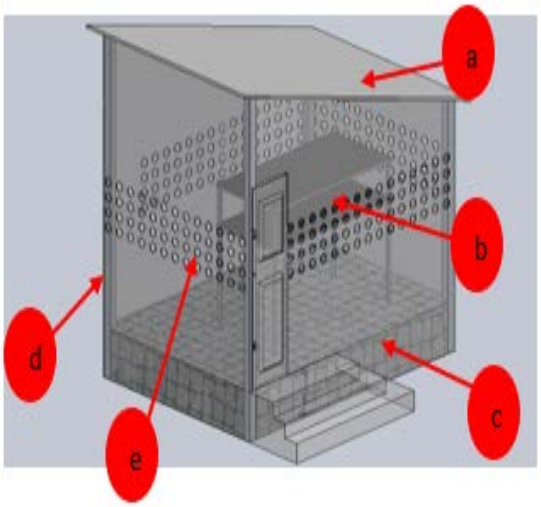

Figure 1. Perspective diagram of the brine solar dryer (a: Plexiglas roof; b: Shelf; c: block of granite; d: Aluminum pole; e: Perforated part)

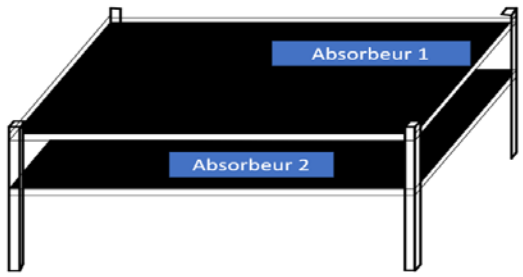

Figure 2. Perspective of an absorber

Inside the greenhouse are two shelves each comprising two drying trays of 1x2 m^2 size covered with a black tarpaulin (absorbent) called geomembrane (Figure 2). The role of the geomembrane is to contain a layer of brine which will then be crystallized.

As the wind is an important parameter in the phenomenon of evaporation, the side walls are perforated to a height of 500 mm to allow natural circulation of the wind through the greenhouse (Figure 1).

For the simulation, the global irradiation on a horizontal plane, the latitude and longitude of the installation site, the ground albedo are downloaded from the PVGIS website **. This allows anyone to redo this study regardless of their geographical position.

2.2. Methodology

Assessing the device's performance means knowing its salt production capacity. However, the rate of evaporation of the water contained in each level of brine is a parameter which makes it possible to quantify the salt produced per day. The DALTON model (1802) makes it possible to determine this evaporation rate, but it has been improved by the Rohwer model (1931) [8].

This present simulation is based on the Rohwer model. But also, the model of Luis and Jordan was used to determine the solar irradiance.

The different steps leading to the determination of the daily salt production are summarized in Figure 3.

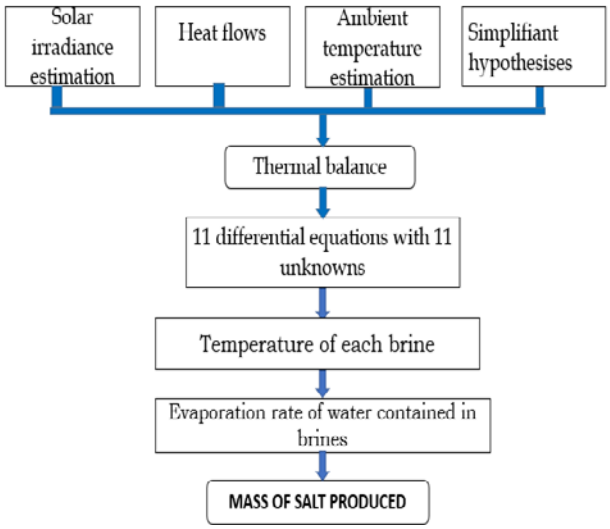

Figure 3. Simulation methodology

• Estimation of Solar irradiance

To estimate solar irradiance, we used the Luis and Jordan model. To work this model needs the simulation position (latitude and longitude), the albedo of the ground, the global irradiation on a horizontal plane and the number of the day of the year. In our case, we chose Abomey-Calavi as the location and January 17 as the simulation day, then we uploaded the global irradiation to PVGIS **. Indeed, the model of Luis and Jordan imposes a representative day for each month of the year, thus the month of January is represented by January 17.

• Estimated ambient temperature

By choosing the location and the day of simulation, we also upload the temperature according to the time on PVGIS.

• Simplifiant hypothesises

- The different components of the solar brine dryer are at different but uniform temperatures.
- There is no temperature gradient through the thickness of the Plexiglas;
- The thermo-physical properties of the solar dryer materials are constants in the operating temperature ranges;
- Heat losses between the granite layer and the ground are negligible because the thickness of the granite layer is significant;
- The celestial vault is considered as a black body;
- Heat exchanges with the aluminum posts are negligible since they are covered with insulating paint;
- Plexiglas does not exchange radiant heat between them because of its low effusivity.

• Heat flows

The different modes of heat transfer in the dryer. The solar brine dryer has a complex energy system where most of the heat transfer modes are involved [9]. It is:

- Radiative exchanges between the granite layer then the other elements of the dryer;
- The radiative exchanges between the brine and the other elements of the dryer;
- Conductive exchanges between the absorbers and the brine layers;
- Convective exchanges between the interior area and the other elements of the dryer;
- Radiative and convective exchanges with the external environment.

Figure 4 illustrates the different heat exchanges involved between the different elements of the solar brine dryer. The solar fluxes absorbed by the different elements have not been shown in this figure so that it is readable. But these flows have been integrated into the different equations. This is the solar flux absorbed by: the roof ($S_{pt}G_{pt}$), the northern vertical wall ($S_{p1}G_{p1}$), the southern vertical wall ($S_{p2}G_{p2}$), the vertical wall is ($S_{p3}G_{p3}$), the western vertical wall ($S_{p4}G_{p4}$), brine S1 ($S_{S1}G_{pt}$) and the layer of rock ($S^*_{roch}G_{pt}$).

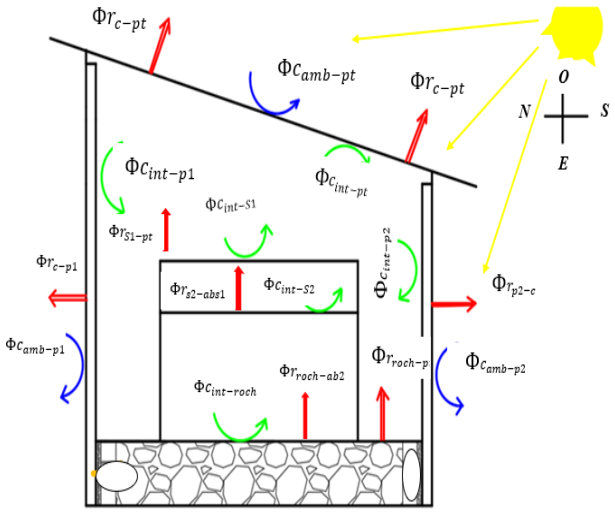

Figure 4. Heat exchanges between the elements of the greenhouse

• Thermal balance [9-14]

The heat flow is proportional to the exchange surface, the exchange coefficient and the temperature difference (Newton).

$$\Phi = S \times h \times \Delta T \tag{1}$$

√ **Thermal balance of the roof (pt)**

$$m_{pt}Cp_p\frac{dT_{pt}}{dt} = S_{pte}G_{pt} + \Phi r_{c-pt} + \Phi c_{amb-pt} + \Phi c_{\text{int}-pt} + \Phi r_{roch-pt} + \Phi r_{pt-S1} \tag{2}$$

S_{pte} : The surface of the outer face of the roof
G_{pt} : Density of solar flux absorbed by the roof
S_{pti} : Ceiling area.

Finally, the thermal balance of the roof (in Plexiglas) is written:

$$\begin{aligned} & m_{pt}Cp_p\frac{dT_{pt}}{dt} \\ & = S_{pte}G_{pt} + S_{pte}h_{r,c-pt}\left(T_c - T_{pt}\right) \\ & + S_{pte}h_{c,amb-pt}\left(T_{amb} - T_{pt}\right) \\ & + S_{pti}h_{c,\text{int}-pt}\left(T_{\text{int}} - T_{pt}\right) \\ & + S^*_{pt}h_{r,roch-pt}\left(T_{roch} - T_{pt}\right) \\ & + S_{S1}h_{r,pt-S1}\left(T_{S1} - T_{pt}\right) \end{aligned} \tag{3}$$

√ **Thermal balance of the northern vertical wall (p1)**

$$m_{p1}Cp_p\frac{dT_{p1}}{dt} = S_{p1}G_{p1} + \Phi c_{amb-p1} + \Phi c_{\text{int}-p1} + \Phi r_{c-p1} \tag{4}$$

S_{p1}: Surface of the north vertical wall
G_{p1} : Density of solar flux absorbed by the northern vertical wall
S^*_{p1}: Surface of the interior face of the north vertical wall in contact with the interior air.

Finally, the thermal balance of the northern vertical wall is written:

$$\begin{aligned} & m_{p1}Cp_p\frac{dT_{p1}}{dt} \\ & = S_{p1}G_{p1} + S_{p1}h_{c,amb-p1}\left(T_{amb} - T_{p1}\right) \\ & + S^*_{p1}h_{c,\text{int}-p1}\left(T_{\text{int}} - T_{p1}\right) + S_{p1}h_{r,c-p1}\left(T_c - T_{p1}\right) \end{aligned} \tag{5}$$

√ **Thermal balance of the southern vertical wall (p2)**

$$\begin{aligned} & m_{p2}Cp_p\frac{dT_{p2}}{dt} \\ & = S_{p2}G_{p2} + \Phi c_{amb-p2} + \Phi c_{\text{int}-p2} + \Phi r_{c-p2} \end{aligned} \tag{6}$$

S_{p2}: Surface of the south vertical wall
G_{p2} : Density of solar flux absorbed by the southern vertical wall
S^*_{p2}: Surface of the interior face of the south vertical wall in contact with the interior air

Finally, the thermal balance of the southern vertical wall is written:

$$\begin{aligned} & m_{p2}Cp_p\frac{dT_{p2}}{dt} \\ & = S_{p2}G_{p2} + S_{p2}h_{c,amb-p2}\left(T_{amb} - T_{p2}\right) \\ & + S^*_{p2}h_{c,\text{int}-p2}\left(T_{\text{int}} - T_{p2}\right) + S_{p2}h_{r,c-p2}\left(T_c - T_{p2}\right) \end{aligned} \quad (7)$$

√ **Heat balance of the eastern vertical wall (p3)**

$$\begin{aligned} & m_{p3}Cp_p\frac{dT_{p3}}{dt} \\ & = S_{p3}G_{p3} + \Phi c_{amb-p3} + \Phi c_{\text{int}-p3} + \Phi r_{c-p3} \end{aligned} \quad (8)$$

S_{p3}: East vertical wall area
G_{p3}: Density of solar flux absorbed by the eastern vertical wall
S^*_{p3}: Surface of the interior face of the vertical wall Is in contact with the interior air

Finally, the heat balance of the eastern vertical wall is written:

$$\begin{aligned} & m_{p3}Cp_p\frac{dT_{p3}}{dt} \\ & = S_{p3}G_{p3} + S_{p3}h_{c,amb-p3}\left(T_{amb} - T_{p3}\right) \\ & + S^*_{p3}h_{c,\text{int}-p3}\left(T_{\text{int}} - T_{p3}\right) + S_{p3}h_{r,c-p3}\left(T_c - T_{p3}\right) \end{aligned} \quad (9)$$

√ **Heat balance of the West vertical wall (p4)**

$$\begin{aligned} & m_{p4}Cp_p\frac{dT_{p4}}{dt} \\ & = S_{p4}G_{p4} + \Phi c_{amb-p4} + \Phi c_{\text{int}-p4} + \Phi r_{c-p4} \end{aligned} \quad (10)$$

S_{p4}: Surface of the West vertical wall
G_{p4}: Solar flux density absorbed by the West vertical wall
S^*_{p4}: Surface of the interior face of the West vertical wall in contact with the interior air

Finally, the thermal balance of the western vertical wall is written:

$$\begin{aligned} & m_{p4}Cp_p\frac{dT_{p4}}{dt} \\ & = S_{p4}G_{p4} + S_{p4}h_{c,amb-p4}\left(T_{amb} - T_{p4}\right) \\ & + S_{p4}h_{c,\text{int}-p4}\left(T_{\text{int}} - T_{p4}\right) \\ & + S_{p4}h_{r,c-p4}\left(T_c - T_{p4}\right) \end{aligned} \quad (11)$$

√ **Heat balance of the rock layer**

$$\begin{aligned} & m_{roch}Cp_{roch}\frac{dT_{roch}}{dt} \\ & = \tau_p S^*_{pt}G_{pt} + \Phi c_{\text{int}-roch} + \Phi r_{roch-pt} + \Phi r_{abs2-roch} \end{aligned} \quad (12)$$

S^*_{pt}: Surface of the granite layer not shaded by the screen
S_{roch}: Upper surface of the rock layer.
S_{ab2}: Lower absorber surface

Finally, the heat balance of the granite layer is written:

$$\begin{aligned} & m_{roch}Cp_{roch}\frac{dT_{roch}}{dt} \\ & = \tau_p S^*_{pt}G_{pt} + S_{roch}h_{c,\text{int}-roch}\left(T_{\text{int}} - T_{roch}\right) \\ & + S^*_{pt}h_{r,roch-pt}\left(T_{pt} - T_{roch}\right) \\ & + S_{ab2}h_{r,ab2-roch}\left(T_{ab2} - T_{roch}\right) \end{aligned} \quad (13)$$

√ **Thermal balance of the upper absorber (ab1)**

$$\begin{aligned} & m_{ab1}Cp_{ab}\frac{dT_{ab1}}{dt} \\ & = \tau_p\tau_s S_{ab1}G_{pt} + \Phi r_{s2-ab1} + \Phi cond_{S1-ab1} + \Phi c_{ab1-\text{int}} \end{aligned} \quad (14)$$

Finally, the heat balance of absorber 1 is written:

$$\begin{aligned} & m_{ab1}Cp_{ab}\frac{dT_{ab1}}{dt} \\ & = \tau_p\tau_s S_{ab1}G_{pt} + S_{ab1}h_{r,S2-ab1}(T_{S2} - T_{ab1}) \\ & + S_{ab1}h_{cond,S1-ab1}\left(T_{S1} - T_{ab1}\right) \\ & + S_{ab1}h_{c,ab1-\text{int}}\left(T_{\text{int}} - T_{ab1}\right) \end{aligned} \quad (15)$$

√ **Lower absorber heat balance (ab2)**

$$\begin{aligned} & m_{ab2}Cp_{ab}\frac{dT_{ab2}}{dt} \\ & = \Phi r_{roch-ab2} + \Phi cond_{S2-ab2} + \Phi c_{ab2-\text{int}} \end{aligned} \quad (16)$$

The heat balance is written:

$$\begin{aligned} & m_{ab2}Cp_{ab}\frac{dT_{ab2}}{dt} \\ & = S_{ab2}h_{r,roch-ab2}\left(T_{roch} - T_{ab2}\right) \\ & + S_{ab2}h_{cond,S2-ab2}\left(T_{S2} - T_{ab2}\right) \\ & + S_{ab2}h_{c,ab2-\text{int}}\left(T_{\text{int}} - T_{ab2}\right) \end{aligned} \quad (17)$$

√ **Heat balance of brine S1**

$$\begin{aligned} & m_{s1}Cp_s\frac{dT_{S1}}{dt} \\ & = \tau_p S_{S1}G_{pt} + \Phi r_{pt-S1} + \Phi cond_{ab1-S1} + \Phi c_{\text{int}-S1} \end{aligned} \quad (18)$$

S_{S1}: The surface of the brine, it is equal to Sab1

The heat balance of brine S1 is written:

$$\begin{aligned} & m_{s1}Cp_s\frac{dT_{S1}}{dt} \\ & = \tau_p S_{S1}G_{pt} + S_{S1}h_{r,pt-S1}\left(T_{pt} - T_{S1}\right) \\ & + S_{S1}h_{cond,ab1-S1}\left(T_{ab1} - T_{S1}\right) \\ & + S_{S1}h_{c,\text{int}-S1}\left(T_{\text{int}} - T_{S1}\right) \end{aligned} \quad (19)$$

√ **Heat balance of brine S2**

$$\begin{aligned} & m_{s2}Cp_s\frac{dT_{S2}}{dt} \\ & = \Phi r_{ab1-S2} + \Phi cond_{ab2-S2} + \Phi c_{\text{int}-S2} \end{aligned} \quad (20)$$

The heat balance of the brine S2 is written:

$$\begin{aligned} & m_{s2}Cp_s\frac{dT_{S2}}{dt} \\ & = S_{S2}h_{r,ab1-S2}\left(T_{ab1}-T_{S2}\right) \\ & +S_{S2}h_{cond,ab2-S2}\left(T_{ab2}-T_{S2}\right) \\ & +S_{S2}h_{c,\text{int}-S2}\left(T_{\text{int}}-T_{S2}\right) \end{aligned} \quad (21)$$

√ **Indoor air heat balance**

$$\begin{aligned} & m_{air}Cp_{air}\frac{dT_a}{dt} \\ & = \Phi c_{pt-\text{int}}+\Phi c_{p1-\text{int}}+\Phi c_{p2-\text{int}}+\Phi c_{p3-\text{int}} \\ & +\Phi c_{p4-\text{int}}+\Phi c_{roch-\text{int}}+\Phi c_{S1-\text{int}}+\Phi c_{S2-\text{int}} \\ & +\Phi c_{ab1-\text{int}}+\Phi c_{ab2-\text{int}}-\frac{Q_{ren\,porte}+Q_{ren\_ouvertues}}{dt} \end{aligned} \quad (22)$$

$Q_{ren\ \text{porte}}$: Heat losses due to air renewal through door openings;

$Q_{ren\ \text{ouvertues}}$: Heat losses due to air renewal through the perforated parts;

The indoor air heat balance is written as:

$$\begin{aligned} & m_{air}Cp_{air}\frac{dT_{\text{int}}}{dt} \\ & = S_{pt}h_{c,pt-\text{int}}\left(T_{pt}-T_{\text{int}}\right)+S_{p1}h_{c,p1-\text{int}}\left(T_{p1}-T_{\text{int}}\right) \\ & +S_{p2}h_{c,p2-\text{int}}\left(T_{p2}-T_{\text{int}}\right)+S_{p3}h_{c,p3-\text{int}}\left(T_{p3}-T_{\text{int}}\right) \\ & +S_{p4}h_{c,p4-\text{int}}\left(T_{p4}-T_{\text{int}}\right) \\ & +S_{roch}h_{c,roch-\text{int}}\left(T_{roch}-T_{\text{int}}\right) \\ & +S_{S1}h_{c,S1-\text{int}}\left(T_{S1}-T_{\text{int}}\right) \\ & +S_{S2}h_{c,S2-\text{int}}\left(T_{S2}-T_{\text{int}}\right) \\ & +S_{ab1}h_{c,ab1-\text{int}}\left(T_{\text{int}}-T_{ab1}\right) \\ & +S_{ab2}h_{c,ab2-\text{int}}\left(T_{\text{int}}-T_{ab2}\right) \\ & -\frac{Q_{ren\,porte}+Q_{ren\_ouvertues}}{dt} \end{aligned} \quad (23)$$

The thermal balance of each element of the greenhouse was made and we obtained 11 differential equations with 11 unknowns. The unknowns being the temperatures of each element of the greenhouse. We used a numerical solution approach to solve these equations (GASS SEIDEL method).

• **Evaporation rate of water contained in brines**

The Rohwer model was used to determine the evaporation rate of water contained in brines [8,15].

$$E = 0,3\times(1+0,6u)\times e^{\left(\frac{17,27.T}{240,97+T}\right)}\times(1-H_r) \quad (24)$$

E: evaporation rate [mm/day]
T: brine temperature [° C]
u: wind speed $[m/s]$
H_r: Relative humidity

3. Simulation Results and Discussions

• **Data availability**

The meteorological data is taken from the PVGis site to make this simulation. [http://re.jrc.ec.europa.eu/pvg_tools/en/tools.html].

The concentration of the brine was obtained by analysis in the LSTEE laboratory of the university of abomey-calavi. This concentration is 39,4 g/L.

This brine is the same as that used with the tarp salt production method.

The depth of the brine is also the same in the case of our simulation as that with the tarp salt production method and is equal to 1 mm.

• **Uncertainty analysis**

The numerical solution tool in this article is MATLAB software. The figures below come from the simulation via MATLAB and the numerical method used is the GAUSS SEIDEL method. The various results in this article have a relative uncertainty of less than 1%

• **BRINE AND ABSORBER TEMPERATURES**

On each absorber, the difference between the temperatures of the absorber and the brine it contains is very small. This is because the thickness of the brine film on each absorber is very thin (Figure 5 and Figure 6).

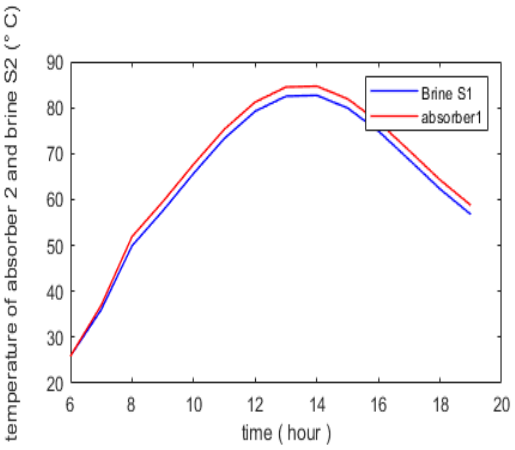

Figure 5. Temperatures of absorber 1 and brine S1 as a function of true solar time (January 17)

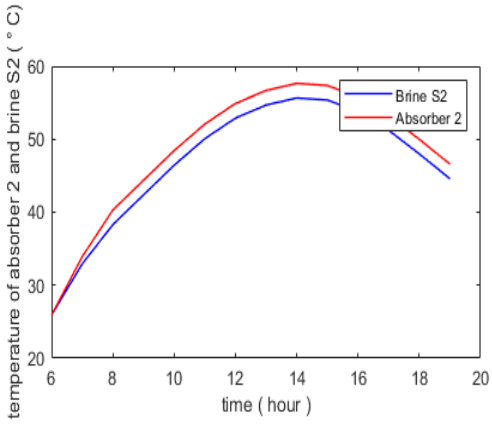

Figure 6. S2 brine temperatures and solar time function of absorber 2 in real life (January 17)

• **Influence of the absorber 1-roof distance on the evaporation rate**

When we vary the distance between the roof and the absorber1, we notice that the more the greenhouse is confined, the faster the evaporation (Figure 7). This is due to the intensification of the greenhouse effect when the volume of the dryer becomes restricted.

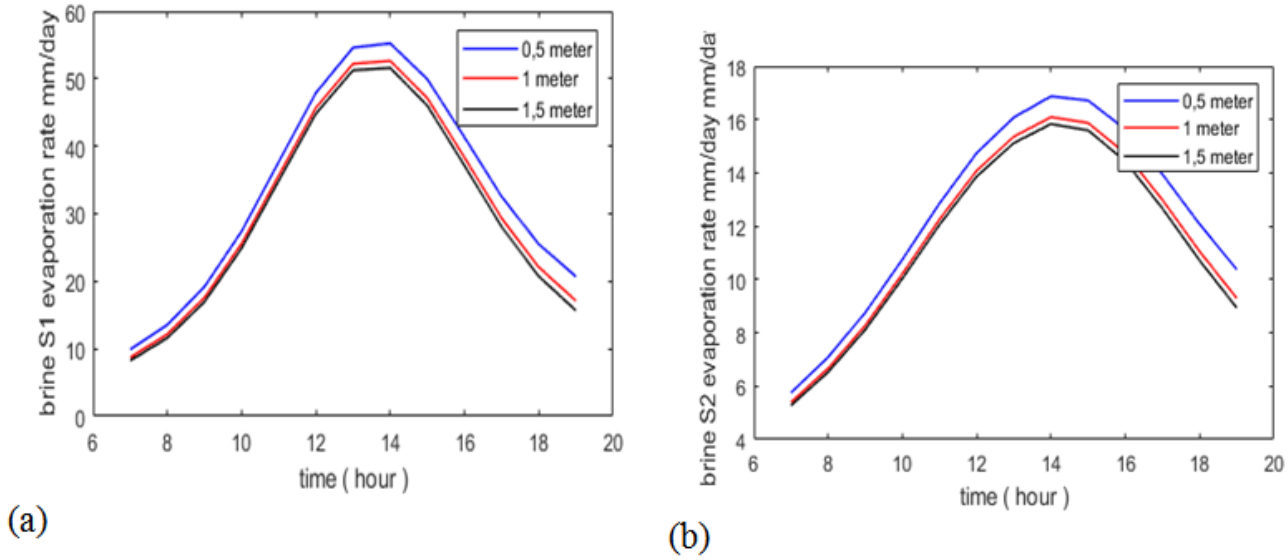

Figure 7. Influence of the roof-absorber distance 1 on the evaporation rate; (a): brine 1; (b): brine 2.

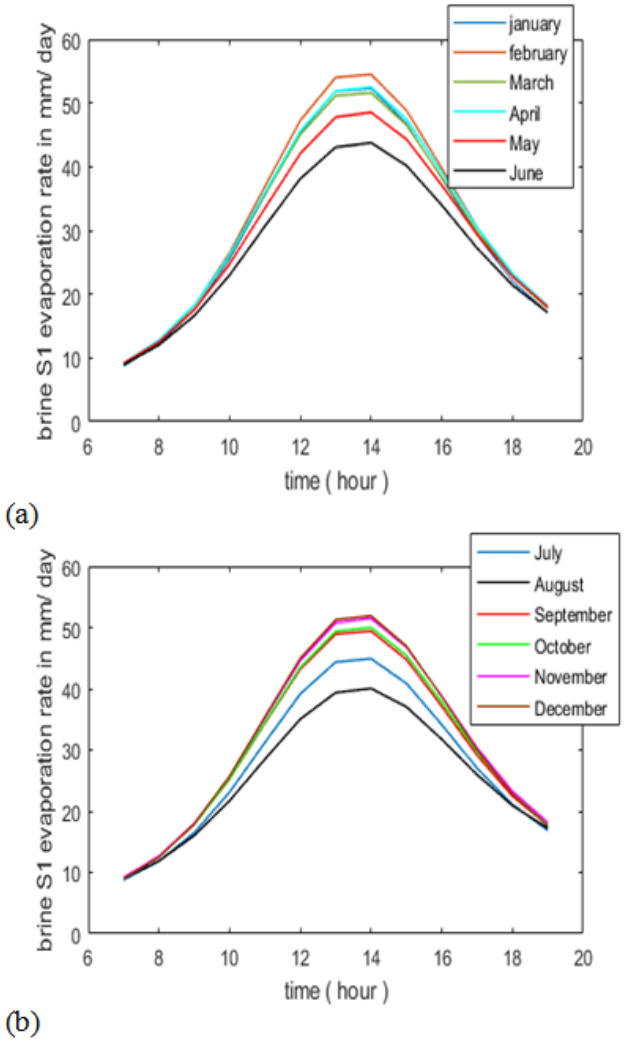

Figure 8. Evolution of the evaporation rate of brine S1 as a function of time for each month of the year: (a) from January to June; (b) from July to December

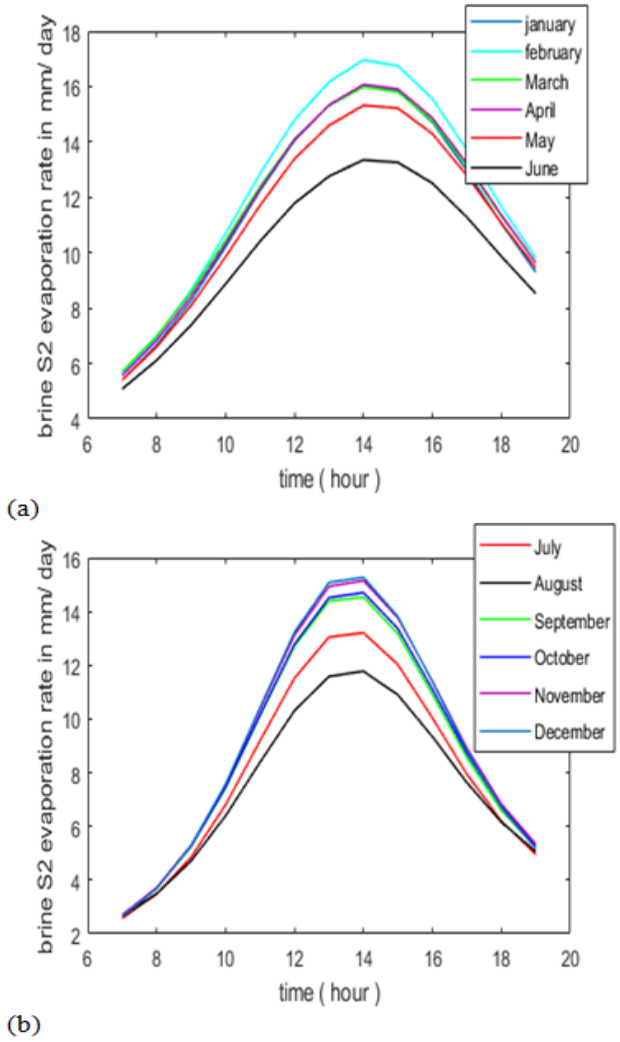

Figure 9. Evolution of the evaporation rate of brine S2 as a function of time for each month of the year: (a) from January to June; (b) from July to December

• **Evaporation rate of the upper brine S1 according to the months of the year**

We can read in Figure 8 the evolution of the evaporation rate of brine S1 as a function of true solar time. Whatever the month of the year, the rate of evaporation of the brine S1 evolves in a Gaussian bell and we notice that the evaporation is rapid between 11 a.m. and 5 p.m. local time. The cause of this is due to the fact that the solar illumination is important in these hours. This figure shows that evaporation is much faster in February, April, January, December and November because these months are the sunniest. On the other hand, evaporation is slow in August, July, June, and May, these months are the least sunny. The average evaporation rate is 28.5 mm/day.

• **Lower brine evaporation rate S2 as a function of the months of the year**

Figure 9 describes the evolution of the evaporation rate of brine S2 as a function of true solar time. Like S1 brine, regardless of the month of the year, the evaporation rate of S2 brine evolves in a Gaussian bell and evaporation is rapid between 11 a.m. and 5 p.m. There is also rapid evaporation in February, April, January, December and November followed by slow evaporation in August, July, June and May. This difference in evaporation rate is caused by the variation in sunlight depending on the month of the year. The average evaporation rate is 11.5 mm/day.

• **MASS OF SALT PRODUCED IN 24h FOR EACH MONTH OF THE YEAR**

The mass of salt produced daily on an absorber is written:

$$m_j = 10^{-3} \times E \times S \times C\left[kg / day\right] \qquad (25)$$

E: Evaporation rate in mm/day
m_j : The mass of salt produced in 24 hours
S: Brine surface [m^2]
C : brine concentration [kg/m^3]

Month	J	F	M	A	M	J
Mass (Kg/day)	7,94	8,2	8,02	8	7,58	6,9
	J	A	S	O	N	D
	6,92	6,44	7,6	7,6	7,62	7,78

The average daily production of the drying greenhouse is 7.55 kg/day.

• **COMPARISON OF THE BRINE DRYING GREENHOUSE AND THE TARP SALT PRODUCTION METHOD**

√ **Daily salt production**

Salt production is 1.4 kg per day with the tarpaulin production method (Field survey as part of FOCUSED-Benin) while this production is 7.55 kg of salt per day with the drying greenhouse brine.

√ **Floor area occupied by production**

The area occupied for a production of 1.4 kg of salt by the method of production by tarpaulin (Field survey as part of FOCUSED-Benin) is 250 m^2 while the brine drying greenhouse uses 12 m^2 to produce 7.55 kg of salt per day.

√ **Ratio mass produced and surface occupied**

The ratio of the mass of salt produced and the surface area occupied is 0.0056 kg/m^2 for the salt production method on a tarp and 0,629 kg/m^2 for brine drying greenhouse.

4. Conclusion

This work is part of the production of sea salt by the action of solar radiation and natural convection of the wind. Our device being a brine drying greenhouse, whose operation is based on the greenhouse effect and the natural convection of the wind to allow full-time salt production.

The objective of this work was to design a solar brine dryer to make salt production sustainable and optimal in the municipality of Sèmè-Kpodji. This objective was achieved following simulation results with a ratio of mass of salt produced and production surface of 0.629 kg/m^2 for the designed dryer against 0.0056 kg/m^2 for the salt production method. on tarpaulin (geomembrane). In addition, the designed device produces the salt full time and the salt produced is not contaminated by sea sand.

Acknowledgements

The authors would like to greatly thank Yann Emmanuel MIASSI and Aubéda MOUSSA from the University of Çukurova (Turkey) for their participation in the proofreading and improvement of the content of the article.

Nomenclature

C_{pi} : Heat capacity *i*, [J / (K.kg)]
E1: Evaporation rate of S1, [mm / day]
E2: Evaporation rate of S2, [mm / day]
G: Absorbed solar flux density [W / m^2]
$\Phi m_{ele1\text{-}ele2}$: Flux exchanged by the heat transfer mode *m* [W]
$hm_{ele1\text{-}ele2}$: Coefficient of heat exchange by mode m between elements *ele1* and *ele2* [W / ($K.m^2$)]
m: Mass of salt produced by evaporation of brine from a single absorber [kg]
m_j: Mass of salt produced daily [kg]
G: Absorbed solar flux density [W / m^2]
$\Phi m_{ele1\text{-}ele2}$: Flux exchanged by the heat transfer mode *m* [W]
$hm_{ele1\text{-}ele2}$: Coefficient of heat exchange by mode m between elements *ele1* and *ele2* [W / ($K.m^2$)]
m: Mass of salt produced by evaporation of brine from a single absorber [kg]
m_j: Mass of salt produced daily [kg]
P_e: Effective pressure [kPa]
P_s: Vapor pressure [kPa]
S_i: Area of an element with index *i* [m^2]
T_i: Element temperature *i* [^oC]
ε: Emissivity
λ: thermal conduction [W/ (K.m)]
Index i, ele1 and ele2
Pt: Plexiglas roof
Pte: exterior roof
Pti: interior roof
Roch: granite rock

Ab: absorber
Abs1: upper absorber
Abs2: lower absorber
S1: upper brine
S2: lower brine
int: interior
c: convection
cond: conduction
r: radiation
s: brine

References

[1] UNIVERS-SEL. Les usages sociaux du sel. Frise chronologique histoire du sel - Inrap. https://www.inrap.fr/dossiers/Archeologie-du-Sel/Qu-est-ce-que-le-sel-/Les-usages-sociaux-du-sel (accessed August 10, 2021).

[2] Archéologie du Sel-Les modes de production. Frise chronologique histoire du sel. Inrap https://www.inrap.fr/dossiers/Archeologie-du-Sel/Qu-est-ce-que-le-sel-/Les-modes-de-production (accessed August 03, 2021).

[3] J. Dossou et al.Amélioration des procédés traditionnels de production de sel alimentaire (NaCI) par l'utilisation d'un distillateur solaire d'eau de mer. Bulletin de la recherche Agronomique du Bénin, Numéro 67, 47-57 (2010).

[4] H. Ouahid. Etude de la performance d'un distillateur solaire par un système de pré-chauffage solaire de l'eau saumâtre. Diplôme de Magister, Université Mentouri Constantine, 2010, p12.

[5] Fatima Sow. Produire du sel solaire sur bâche pour ne pas détruire les mangroves | Espaces naturels. http://www.espaces-naturels.info/produire-sel-solaire-sur-bache-pour-ne-pas-detruire-mangroves (Accessed August 08, 2021).

[6] M. BANI. Concevoir un système énergétique autonome dénommé distillateur solaire pour une production de sel de cuisine et d'électricité. Mémoire d'ingénieur de conception, Université d'Abomey-Calavi, EPAC, p.7(2019).

[7] K. N'TSOUKPOE. Effet des angles d'inclinaison de d'orientation des capteurs solaires sur leur production : cas des capitales des pays d'Afrique de l'Ouest et du Centre. Laboratoire Energie Solaire et Economie. Institut International de l'Ingénieur de l'Eau et de l'Environnement.p1, (2017).

[8] Nicolas Rodriguez. Chapitre 4 - Évaporation et interception. https://echo2.epfl.ch/e-drologie/chapitres/chapitre4/chapitre4.html (2021).

[9] H.Nora. Contribution à l'étude du comportem²ent thermique d'un cuiseur solaire boite installé dans le Nord de l'Algérie. Mémoire de Master, Université Mouloud Mammeri de Tizi-Ouzou, p 34-56 (2013).

[10] A. MOUMMI et al. Estimation du rayonnement solaire par deux approches semi empiriques dans le site de Biskra. Centre Universitaire de Béchar-Algérie, p83 (2006).

[11] H. OLUBI .Amélioration du séchage des amandes de karité dans le centre et le nord Benin, conception participative et dimensionnement d'un séchoir solaire indirect a effet de serre. Mémoire d'ingénieur de conception, Université d'Abomey-Calavi, EPAC,71-91 (2010).

[12] A. Boussalia. Contribution à l'étude de séchage solaire de produits agricoles locaux. Diplôme de Magister, Université Mentouri-Constantine, 41-72 (2010).

[13] J. NEBIE et al. Modelisation des paramètres d'un cuiseur solaire de types boite sous les conditions météorologiques du Burkina Faso. Journal de physique de la SOAPHYS.p3 (2019).

[14] C. AHOUANNOU. Etude du séchage de produits agroalimentaires tropicaux: application au manioc, gingembre, gombo et piment. Thèse de doctorat, Université Nationale du Bénin. (2001).

[15] S. MOKDAD. Contribution à la détermination de la courbe de pression de vapeur saturante de l'eau pure dans la plage de -80°C à +100°C, avec une très haute exactitude. HAL. p67. (2012).